JOURNAL OF Applied Polymer SCIENCE

Polystyrene/Attapulgite Nanocomposites Prepared via *In Situ* Suspension Polymerization with Redox Initiation System

Haicun Yang,[1] Liu Zhang,[2] Wenzhong Ma,[2] Hongting Pu,[1] Fanghong Gong[2]

[1]Institute of Functional Polymers, School of Materials Science and Engineering, Tongji University, Shanghai 201804, People's Republic of China

[2]School of Materials Science and Engineering, Changzhou University, Changzhou 213164, People's Republic of China

Correspondence to: H. Pu (E-mail: puhongting@tongji.edu.cn) and F. Gong (E-mail: fhgong@cczu.edu.cn)

ABSTRACT: A series of polymer–clay nanocomposites consisting of polystyrene (PS) and attapuglite (ATP) were prepared successfully. First, silane coupling agent containing aromatic tertiary amine groups was synthesized to functionalize ATP (M-ATP). Then, PS nanocomposites with varied clay loadings were prepared via *in situ* suspension polymerization process with a redox initiation system consisting of aromatic tertiary amine and benzoyl peroxide. The synthesis of silane coupling agent and functionalization of ATP were confirmed by Fourier transform infrared spectroscopy, proton nuclear magnetic resonance spectra, and X-ray photoelectron spectroscopy. Mechanical properties, morphology, thermal stability, and rheological behavior of nanocomposites were investigated to illuminate the effects of M-ATP on the structure and properties of nanocomposites. Field-emission scanning electron microscope images revealed an ideal dispersion of M-ATP and an enhanced toughness of nanocomposites. The improved interface interaction between M-ATP and PS matrix endowed the nanocomposites with outstanding mechanical properties and thermal stability. The formation of hybrid network in the nanocomposites containing 3 wt % M-ATP resulted in higher complex viscosity (η^*), storage modulus (G'), and lower loss factor (tanδ) compared with the pristine PS and PS/ATP nanocomposites. © 2014 Wiley Periodicals, Inc. J. Appl. Polym. Sci. **2015**, *132*, 41567.

KEYWORDS: clay; composites; polystyrene; properties and characterization; radical polymerization

Received 4 June 2014; accepted 28 September 2014

DOI: 10.1002/app.41567

INTRODUCTION

As a new class of material with at least one ultrafine phase dimension, polymer nanocomposites have attracted great interest in recent years because of their tremendously improved properties and significant application in industry. For example, the fill of inorganic nanoparticles can exhibit remarkable improvement in mechanical, thermal, and other excellent properties when compared with pure organic polymer materials because of the large interfacial area per unit volume.[1–4] Polymer materials such as poly(ethylene terephthalate),[5] polyacrylonitrile,[6] polyamide-6,[7] epoxy resins,[8] polypropylene,[9] polyurethane,[10] and waterborne polyurethane[11] have been widely used as matrices in the design of nanocomposites. Dispersed phase that has been used to enforce polymer matrix includes nano-SiO_2,[12] nano-clay,[13] carbon nanotubes (CNTs),[14] metallic nanopowders,[15] and so on. Generally, there are three major methods to prepare nanocomposites: (1) inorganic particles are dispersed in polymer melt or solution directly.[16,17] (2) Particles are distributed in the monomer after modification, and then an *in situ* polymerization is used.[18,19] (3) Precursors are mixed with polymer solution, followed by a sol–gel process.[20,21] The main purpose for above three methods is to improve the interfacial interaction between particles and polymer matrix. It has been proved that a homogeneous dispersion can be formed in nanocomposites by *in situ* polymerization and sol–gel processes. For a decade since the pioneering work on nylon/montmorillonite (MMT),[22] different kinds of polymer/MMT nanocomposites have been synthesized successfully due to that monomers can diffuse into MMT layers and form intercalated or exfoliated nanocomposites through *in situ* intercalation–polymerization.[23,24] Intercalated polystyrene (PS)–clay nanocomposites have been prepared via melt intercalation and *in situ* intercalation–polymerization in presence of organophilic clay by several researchers.[25–29]

Attapulgite (ATP) is a kind of hydrated magnesium aluminum with the structural formula of $Si_8O_{20}Mg_5(Al)(OH)_2(H_2O)_4{\cdot}4H_2O$ and has a fibrous morphology, which is different from layered silicates used in polymer nanocomposites.[30] ATP has excellent mechanical, thermal properties, together with larger surface area and stronger absorption capacity than other clay minerals. These special properties endow ATP a wide

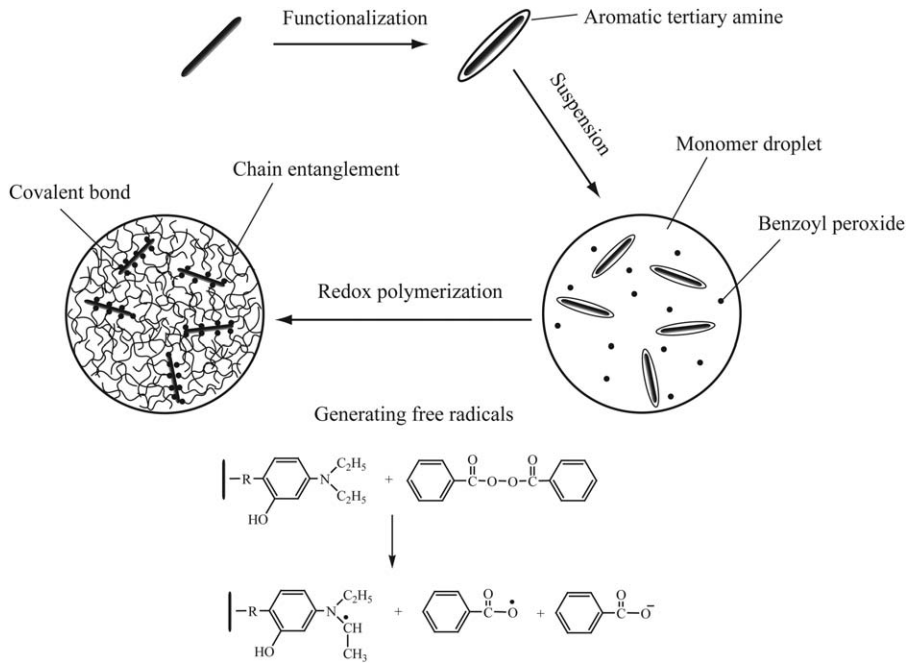

Figure 1. Formation of hybrid network via *in situ* suspension polymerization in the presence of functionalized ATP.

application in clay mineralogy,[31] environmental protection,[32] and catalyst engineering.[33] It has also drawn much attention in the preparation of polymer nanocomposites[34–37]; however, as a polymer reinforcing agent with only a few reports devoted to the composites of polystyrene. As is well known, the major drawbacks of PS are its poor native mechanical properties such as fragileness, the fundamental properties need to be fulfilled before it can exhibit the major useful service properties. Liu et al.[38] synthesized PS/ATP nanocomposites via *in situ* bulk polymerization by using a long-chain quaternary ammonium salt surfactant, results showed that the thermal stability of the nanocomposites was enhanced with the increase of additional ATP. The similar nanocomposites prepared via *in situ* copolymerization of styrene and polymerizable organophilic ATP have been reported by Yang et al.,[39] where silane surface treatment of ATP was more effective on strengthening and toughening. However, the weak interconnection between two phases may result in insufficient polystyrene chains to wet the ATP surface, which prevented the materials from achieving high properties.

In the current work, as shown in Figure 1, a kind of functionalized silane coupling agent was synthesized to anchor reducing aromatic tertiary amine groups on the surface of ATP (M-ATP). Then, nanocomposites were prepared via *in situ* suspension polymerization, in which free radicals were generated by benzoyl peroxide in combination with the reducing ATP.[40] Thus, an organic/inorganic hybrid network based on covalent bonds and chain entanglements was formed in nanocomposites by means of this grafting from method. The dispersion, mechanical properties, thermal properties, and rheological behavior were investigated in detail.

EXPERIMENTAL

Materials

Attapulgite (ATP) was supplied by Jiangsu NDZ Technology Co. (Jiangsu, China). It was activated in 1 mol/L of hydrochloric acid for a day and then dried in a vacuum at 120°C for 36 h before use. 3-Aminopropyltriethoxysilane (APTES, 98%) and *p*-toluenesulfonic acid (PTSA, AR) were purchased from Aladdin-reagent Co. (Shanghai, China). PTSA was purified by recrystallization from toluene. 4-(Diethylamino) salicylaldehyde (DEAS, 99%) was provided by Chengdu Xiya Chemical Technology Co. (Sichuan, China). Styrene (St, AR) and benzoyl peroxide (BPO, CP) were obtained from Sinopharm Chemical Reagent Co. (Shanghai, China), styrene was purified by passing through a column filled with basic alumina to remove inhibitors, and BPO was purified by recrystallization from chloroform. Poly(vinyl alcohol) (PVA) (degree of polymerization 1750 ± 50, degree of hydrolysis 88%) and sodium dodecylbenzene sulfonate (SDBS) were brought from Lingfeng Chemical Reagent Co. (Shanghai, China) and prepared separately to 5 wt % aqueous solution and 0.2 wt % aqueous solution. Calcium-trihydroxy phosphate (TCP) and sodium sulfate (Na_2SO_4) were used as received. All organic solvents were of analytical grade and used after dehydration.

Synthesis of Silane Coupling Agent Containing Aromatic Tertiary Amine Groups

The silane coupling agent containing aromatic tertiary amine groups was synthesized by Schiff Base reaction of primary amine and aldehyde groups. A total of 4.83 g DEAS, a catalytic amount of PTSA, 50 mL *N*,*N*-dimethylacetamide (DMAC) and 125 mL benzene were added into a thoroughly dried three-necked round-bottom flask equipped with magnetic stir bar, addition funnel (100 mL), thermometer, water segregator, and condenser tube. The solution thus obtained was heated at reflux in an oil bath. Then, 5.53 g APTES was dissolved in 25 mL DMAC, and this solution was added drop-wise into the flask via the addition funnel in a period of 30 min. The Schiff Base reaction was performed under reflux for 16 h. After reaction, the flask was cooled down to room temperature and solvent

Table I. Preparation Ingredients of Nanocomposites

Sample code	1	2	3	4	5	6	7	8	9
0.2% SDBS solution (mL)	5	5	5	5	5	5	5	5	5
Na_2SO_4 (g)	0.5	0.5	0.5	0.5	0.5	0.5	0.5	0.5	0.5
TCP (g)	0.3	0.3	0.3	0.3	0.3	0.3	0.3	0.3	0.3
5% PVA solution (mL)	15	15	15	15	15	15	15	15	15
Styrene (g)	40	40	40	40	40	40	40	40	40
ATP (g)	—	0.2	0.4	0.6	1.2	—	—	—	—
Modified ATP (g)	—	—	—	—	—	0.2	0.4	0.6	1.2
Deionized water (mL)	150	150	150	150	150	150	150	150	150
BPO (g)	0.2	0.2	0.2	0.2	0.2	0.2	0.2	0.2	0.2
Additional TCP (g)	0.3	0.3	0.3	0.3	0.3	0.3	0.3	0.3	0.3

was removed by vacuum distillation. After being dried with anhydrous sodium sulfate overnight, the product was isolated by distillation under reduced pressure, and fractions that were croci in color were collected and kept in a dark and preferably dry place at room temperature (yield of 69%).

Surface Immobilization of Aromatic Tertiary Amine Groups

The immobilization of aromatic tertiary amine groups was realized by the reaction of alkoxy with hydroxyl on the surface of ATP. A typical procedure was as follows: 2.0 g ATP was dispersed in 150 mL toluene in a 250-mL three-necked round-bottom flask under ultrasonic vibration and strong stirring condition for 30 min. Then, 4.0 g synthetic silane coupling agent was added into the flask. The immobilization was performed with mechanic stirring and reflux for 10 h. The solid product was separated by centrifugation, and washed three times with toluene to remove absorbed coupling agent. The final product functionalized ATP was dried in vacuum at 50°C. The amount of aromatic tertiary amine groups of unit mass was 1.68 mmol/g calculated by element analysis.

Preparation of Nanocomposites via *In Situ* Suspension Polymerization

In situ suspension polymerization of styrene in the presence of M-ATP was performed by using BPO as an oil-soluble oxidant. The detailed recipes for the synthesis of nanocomposites were listed in Table I, and the typical preparation procedure was performed according to the method described previously.[41] First, 150 mL deionized water, 0.5 g Na_2SO_4, and 5 mL 0.2 wt % SDBS were mixed in a 250-mL three-necked round-bottom flask equipped with mechanical stir bar and condenser tube, and then 15 mL 5 wt % PVA solution was added. The mixture was kept under mechanical stirring in an oil bath at 50°C for 20 min. Subsequently, M-ATP was dispersed in 40 g of styrene with ultrasonic vibration for 15 min to produce a homogeneous suspension, and then 0.2 g BPO was dissolved in this mixture. After that, the above mixture was added drop-wise into the flask. When a stable oil/water suspension system was formed, the flask was heated to 65°C gradually. The polymerization was performed under continuous mechanical stirring and 0.3 g TCP was added during polymerization to maintain a stable polymerization system. The final products were filtrated, washed, and dried at 70°C in an air-blast drying oven. The obtained nanocomposites were compression molded at 180°C in a plate vulcanization machine for 10 min (XLB-D350×350×2, Changzhou, China). Specimens with different dimensions in thickness were cut from plaques for the different measurements.

Characterization

Fourier transform infrared spectra were collected by an Avatar 370 FTIR spectrometer (FTIR, Nicolet, USA). A wavelength range of 500–4000 cm^{-1} and a resolution of 2 cm^{-1} were used. ^1H NMR spectra was recorded by an Avance III 400 MHz Nuclear magnetic resonance spectrometer (NMR, Bruker, Switzerland) using $CDCl_3$ as a solvent and TMS as internal standard. X-ray photoelectron spectroscopy was collected on an Escalab 250Xi spectrometer (XPS, Thermo Fisher, USA) in an ultra high vacuum with Al Kα radiation.

Tensile and flexural tests were performed at room temperature on a WDT-10 universal material tester (Shenzhen, China). Tensile properties were performed according to the ASTM D638 standard method at a crosshead speed of 50 mm/min. Flexural properties were performed according to the ASTM D790 standard method with the press down rate of 1.2 mm/min. Impact strength was measured according to the ASTM D256 standard method on an XJU- 22 Izod impact tester (Chengde, China). The morphology of fracture surface was studied using a SUPRA55 field emission scanning electronic microscope (FESEM, Zeiss, Germany). All the specimens were coated with gold before viewing. Thermogravimetric results were obtained with a TG209 F3 system (TGA, Netzsch, Germany) within the temperature range of 50–850°C at a heating-up rate of 10°C/min. A sample weight of about 10 mg was used and nitrogen at a rate of 50 mL/min was used as the purging gas. Rheological measurements were performed on a MCR301 rotational rheometer (Anton Paar, Germany) at 200°C, using a parallel plate geometry (50 mm diameter) with a gap between the two plates of 1 mm.

RESULTS AND DISCUSSION

Synthesis of Silane Coupling Containing Aromatic Tertiary Amine Groups

The FTIR spectra of silane coupling agent is recorded in a liquid state using KBr disc technique by coating method under

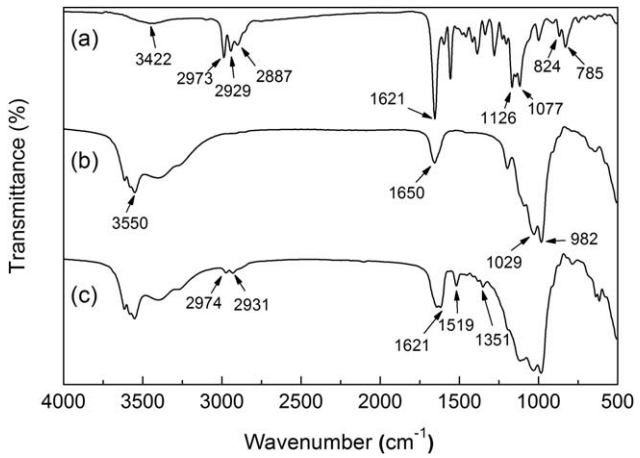

Figure 2. FTIR spectra of (a) silane coupling agent, (b) ATP, and (c) M-ATP.

dry condition, and the result is shown in Figure 2(a). The broadened peak located at 3422 cm^{-1} is due to the stretching vibration of phenolic hydroxyl group (—OH_{phen}),[42] the peaks at 2973, 2929, and 2887 cm^{-1} are assigned to the stretching vibration of C—$H_{aliphatic}$ and the absorption peaks at 824, 785 cm^{-1} are attributed to C—$H_{aromatic}$. The stretching vibration of Si—O—C gives two peaks at 1077 and 1126 cm^{-1}, and the characteristic peak at 1621 cm^{-1} attributed to C=N of Schiff bass confirms that silane coupling with aromatic tertiary amine groups was synthesized successfully.[43] ^{1}H NMR (400 MHz, $CDCl_3$): δ: 7.91 (1H, s, —N=CH—), 6.94–6.96 (1H, d, ArH), 6.12–6.14 (1H, d, ArH), 6.04 (1H, s, ArH), 3.79–3.83 (6H, t, —CH_2—), 3.41–3.48 (2H, t, —CH_2—), 3.33–3.38 (4H, t, —CH_2—), 1.73–1.80 (2H, t, —CH_2—), 1.19–1.24 (9H, t, —CH_3), 1.15–1.18 (6H, t, —CH_3), 0.65–0.69 (2H, t, —CH_2—) (Figure 3).

Surface Functionalization of ATP with Aromatic Tertiary Amine Groups

FTIR analysis of ATP and M-ATP was performed in a solid state with KBr pellet method. In the FTIR spectra of ATP [Figure 2(b)], the absorption band at 3550 cm^{-1} is assigned to the hydroxyl groups of coordinated water in the tunnel of ATP. The peak at 1650 cm^{-1} is attributed to hydroxyl groups of zeolite water.[44] The two sharp absorption peaks at 1029 and 982 cm^{-1} correspond to the stretching vibration of Si—O—Si bond.[45] Compared with the spectra of pure ATP, in the spectra of M-ATP [Figure 2(c)], the peak at 1519 cm^{-1} represents the skeletal vibration of aromatic ring. The grafting of silane coupling agent on the surface of ATP is confirmed by the new absorption peaks of C—H stretching vibrations at 2974, 2931, and 1351 cm^{-1}. Furthermore, because of overlapping with the characterization peak at 1650 cm^{-1} of ATP, a weak but visible peak at 1621 cm^{-1} assigned to C=N stretching vibration can be observed. These experimental findings suggest that silane coupling agent was reacted with the hydroxyl groups on the surface of ATP.

XPS was used to investigate the surface chemical composition of ATP and the results are shown in Figure 4. In the wide-scan spectra of pure ATP [Figure 4(a)], the dominated signals are attributed to silicon (103.3 eV, Si2p; 154.4 eV, Si2s), magnesium (1304.4 eV, Mg1s), carbon (284.9 ev, C1s), oxygen (531.8eV, O1s) elements. For the spectra of modified ATP [Figure 4(b)], representative peaks for the Si2s and Si2p are also observed, and a new peak of nitrogen (399.2 eV, N1s) is clearly observed. What's more, the surface carbon content is increased after modification, which results from the high carbon content of silane coupling agent. In the narrow scan C1s core-level spectra of modified ATP [Figure 4(c)], the BE values of 283.3, 284.7, 285.7, and 286.3 eV are assigned to the C—Si, C—C/C=C/C—H, C—N, and C=N/C—O, respectively.[46–48] In addition, the C1s π-π^* shake-up energy region of benzene ring can be seen at about 289–296 eV. In the narrow scan N1s core-level spectra of modified ATP [Figure 4(d)], the BE value of 398.8, 399.8, and 401.3 eV are assigned to N—$C_{aromatic}$, N=C, and N—$C_{aliphatic}$.[49] These results indicate that ATP has been functionalized with aromatic tertiary amine groups successfully.

Mechanical Properties

Mechanical properties of pure PS, PS/ATP, and PS/M-ATP nanocomposites are measured and summarized in Figure 5. It can be seen from Figure 5(a), the highest tensile strength is 67.6 Mpa obtained from loading of 3 wt % M-ATP, which is 65% higher than that of pristine PS. The introduction of aromatic tertiary amine groups on the surface of ATP leads to the parallel alignment of aromatic rings in the PS chains that conduces to the effective load transfer between the ATP surface and PS matrix.[50] Therefore, PS/M–ATP nanocomposites present the higher tensile strength. Similar to the behavior found for tensile strength, the enhancement of impact strength is significant for PS/M-ATP nanocomposites. A maximum improvement of about 51% in the specimens with 3 wt % loading of M-ATP can be observed [Figure 5(b)]. For brittle materials such as polystyrene, flexural testing is a meaningful approach to measure the mechanical properties. As shown in Figure 5(c), flexural strength of PS/M-ATP nanocomposites is improved with the addition of M-ATP. It should be noticed that around 48% enhancement is achieved by introducing 3 wt % M-ATP into PS matrix. Figure 5(d) shows the flexural

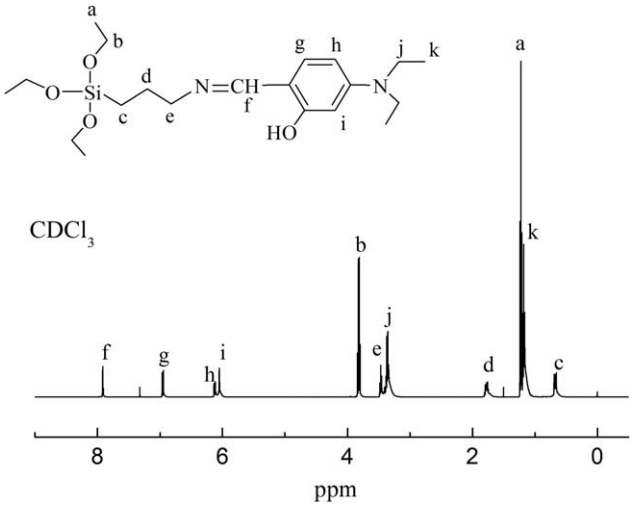

Figure 3. ^{1}H NMR spectra of silane coupling agent.

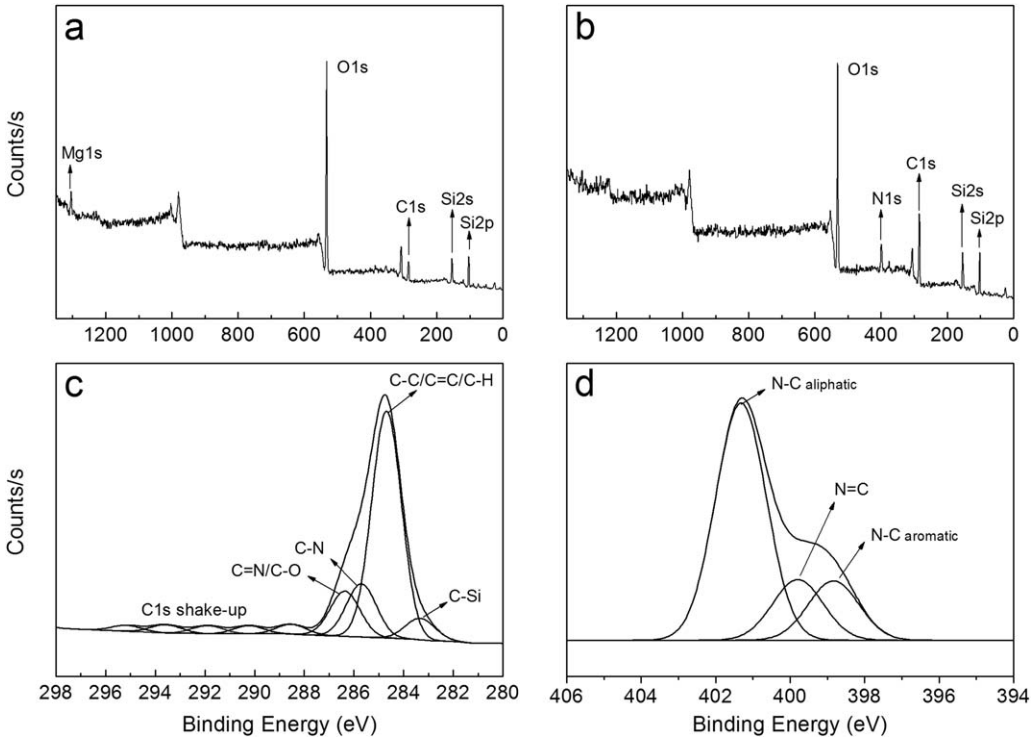

Figure 4. XPS full-scan spectrum of (a) ATP, (b) M-ATP, (c) C1s core-level spectra, and (d) N1s core-level spectra of M-ATP.

modulus of PS/ATP and PS/M-ATP nanocomposites with different loadings. A largest increase in flexural modulus is found at the lower concentration of ATP or M-ATP. The flexural modulus of PS/ATP and PS/M-ATP nanocomposites increases about 25 and 38%, respectively, than pristine PS by 1.5 wt % loading of ATP and M-ATP.

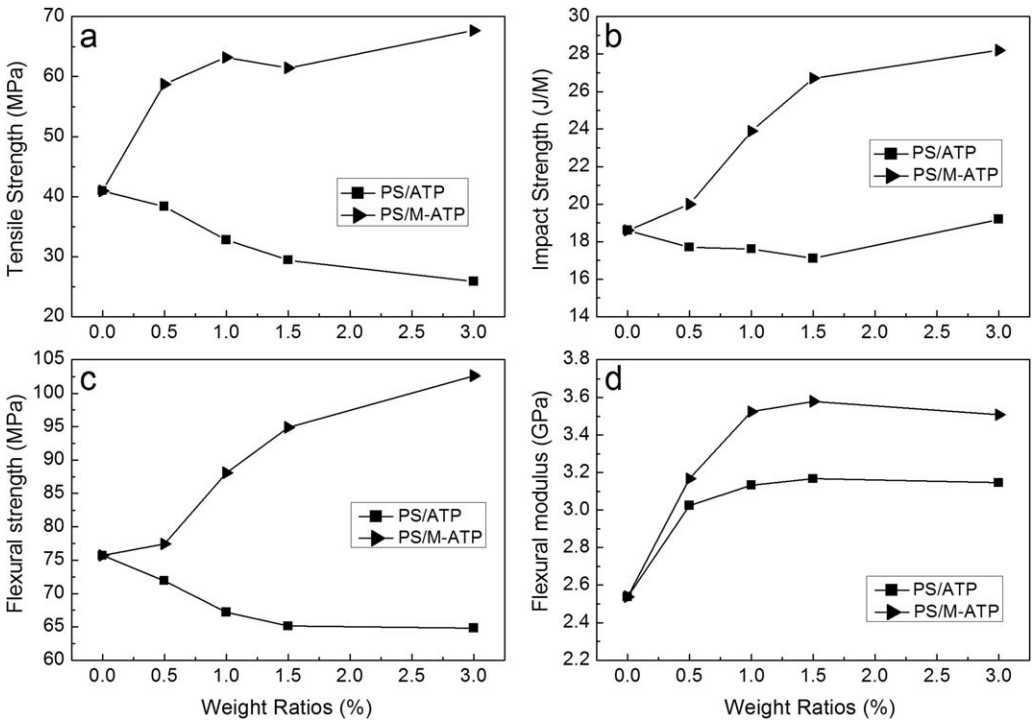

Figure 5. Mechanical properties of both pristine PS and nanocomposites containing various weight ratio of ATP: (a) tensile strength, (b) impact strength, (c) flexural strength, and (d) flexural modulus.

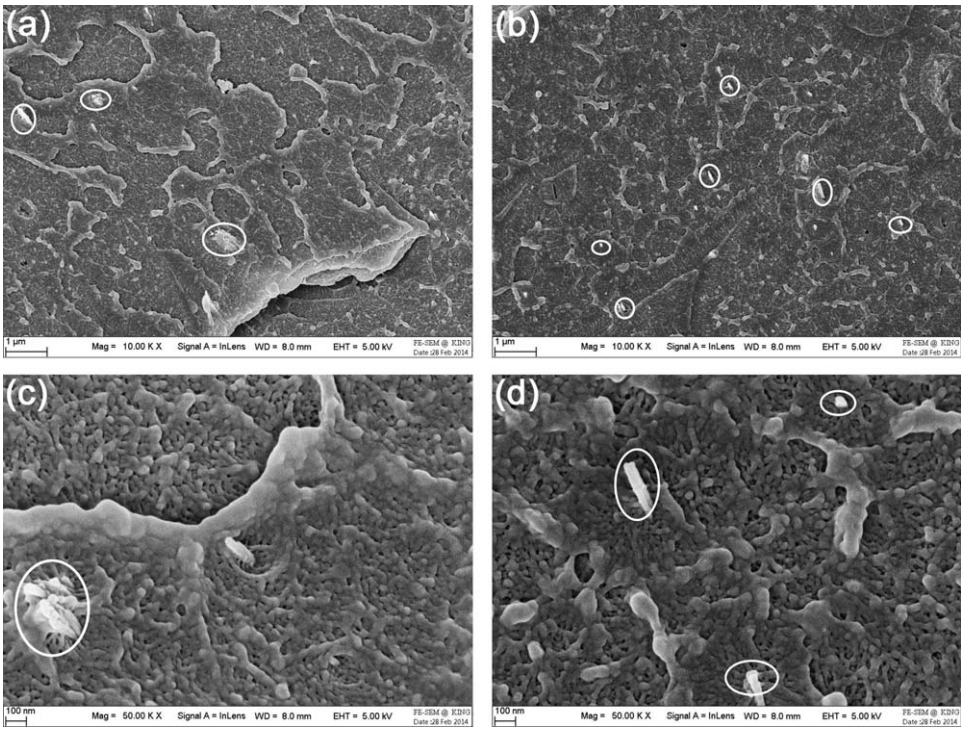

Figure 6. The aggregation of ATP and M-ATP observed by FESEM in (a, c) 1 wt % PS/ATP and (b, d) 1 wt % PS/M-ATP.

In general, the interaction between the two phases is responsible for the improved mechanical properties. An effective hybrid network is most expected in nanocomposites, which is achieved by functionalizing ATP with aromatic tertiary amine groups and the subsequent *in situ* suspension polymerization. The improved adhesion between ATP and PS matrix leads to an effective stress transfer from the weaker PS matrix to the stronger ATP nanorod crystal. Meanwhile, the dispersion should be taken into account to avoid stress concentration. As proved in Figure. 6, larger ATP clusters are observed in 1 wt % PS/ATP, which reflects the worse distribution. However, the agglomeration is alleviated remarkably in PS/M-ATP nanocomposites.

Morphology Observation

The typical impact fracture surfaces of pristine PS and nanocomposites with 3 wt % loading of clay are shown in Figure 7. The fracture surface of PS is composed of several small pieces of relatively smooth surfaces, which suggests a fragile fracture. In contrast, PS/ATP exhibits a slightly rough fracture surface resulting from the plastic flow during damaging, which indicates the toughness of nanocomposites is improved. After surface functionalization, the fracture surface of PS/M-ATP nanocomposites becomes rougher, because M-ATP can play as chemical cross-linking sites in the presence of hybrid network, and thus deflect cracks pathway effectively.

Thermal Properties

TGA and DTG curves of pristine PS and nanocomposites are shown in Figure 8. All samples are degraded with one weight-loss stage occurs during degradation. When ATP or M-ATP is added, thermal decomposition temperature of nanocomposites shifts to a level obviously higher than that of pure PS, suggesting that thermal stability is enhanced. As shown in DTG curves of nanocomposites, the intensity of the peaks at 370–450°C decreases markedly by inducing ATP or M-ATP particles, which corresponding to the analysis of TG curves. Meanwhile, a slightly higher decomposition rate of PS/M-ATP nanocomposites is observed in comparison with that of PS/ATP, which is associated with the decomposition of the organic component on the surface of M-ATP. These results may be attributed to the physical barrier effect of ATP in the polymeric network, where ATP impedes the diffusion of decomposition reaction in nanocomposites.[51,52] Moreover, the physical barrier effect may be more pronounced in the PS/M–ATP nanocomposites due to the effective organic/inorganic hybrid network formed of physical and chemical cross-linking.

Rheological Properties

Rheological analysis is an efficient method to predict the processing behavior and microstructure of nanocomposites. The dependence of complex viscosity on the angular frequency of pristine PS, PS/ATP, and PS/M-ATP nanocomposites is shown in Figure 9. Each curve can be divided into two stages. In the first stage, the decrease of complex viscosity as function of frequency is slow, approximating to the Newtonian fluid, whereas in the second stage, the complex viscosity decreases sharply, exhibiting a typical shear thinning behavior. This phenomenon is attributed to the rate of polymer chains disentanglement and orientation. It should be noted that the complex viscosity of PS/ATP decreases as incorporating small quantity of ATP (1 wt %) and then increases as further elevating concentration of ATP. This observed drop in complex viscosity at the low content filler

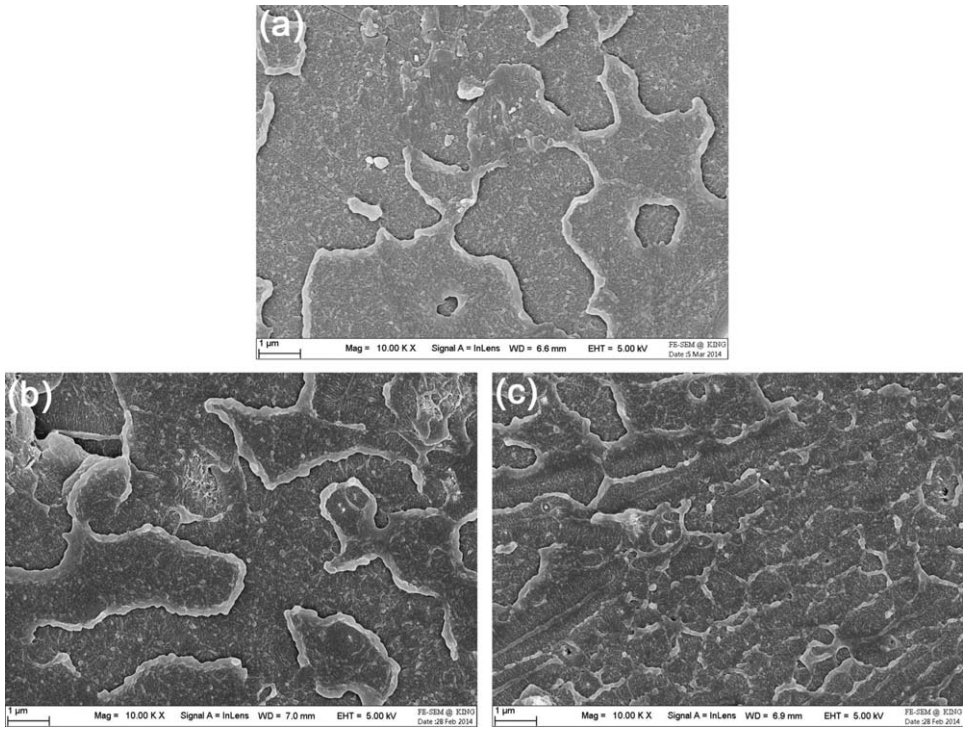

Figure 7. FESEM images of fracture surface of (a) pristine PS, (b) 3 wt % PS/ATP, and (c) 3 wt % PS/M-ATP.

has been reported elsewhere.[53,54] The explanation provided for the viscosity drop is that the orientation of the rigid nanofillers under shear may disturb the entanglement of the polymer chains and apparently facilitate the motion of polymer chains. Whereas, it is interesting to find that at the same content (3 wt %), M-ATP increases the complex viscosity of nanocomposites significantly. It has been reported that the orientation of rigid nanoparticles to the shear force is much faster than relatively soft polymer chains.[55] In PS/M-ATP nanocomposites, ungrafted–grafted chain entanglements obstruct the orientation of ATP and thereby the contribution of the oriented ATP on the disentanglement of PS chains is limited. Generally, in composites systems, disentanglement and friction are the two main factors that affect the complex viscosity of composites. According to the analysis above, the disentanglement effect is more obvious in this system.

Changes in complex viscosity of composites are primarily caused by a marked increase in the storage modulus (G'). As shown in Figure 10, the values of G' of all samples increase with the frequency and the increase of 3% PS/M-ATP nanocomposites is more significant at the low frequency. As 3 wt % of M-ATP is loaded, the density of hybrid network is also increased, and a rubber-like interconnected structure will be probably formed, which restrains the long-range motion of polymer chains and thereby results in the increase of G'.

Loss factor ($\tan\delta = G''/G'$) is used to characterize the viscoelasticity of a material, the lower $\tan\delta$ means that the material exhibits relatively more solid-like behavior.[56] Figure 11 shows the relationship between the angular frequency and the $\tan\delta$ for pristine PS and different nanocomposites. The loss factor of nanocomposites containing 1 wt % of ATP is increased

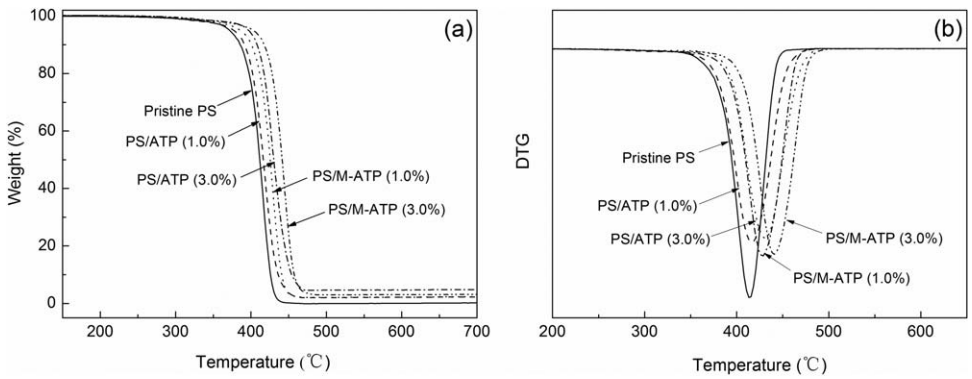

Figure 8. Thermogravimetric curves of pristine PS and PS nanocomposites: (a) TG curves and (b) DTG curves.

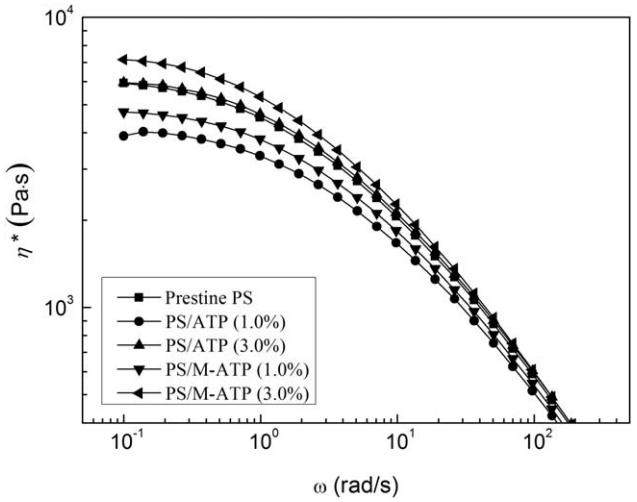

Figure 9. Dependence of complex viscosity on frequency for pristine PS and nanocomposites.

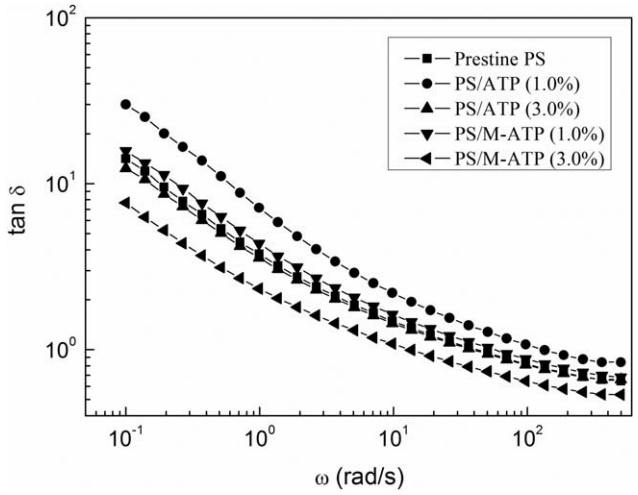

Figure 11. Dependence of tan(δ) on frequency for pristine PS and nanocomposites.

compared with the pristine PS, probably indicating that the mobility of polymer chains is easier. Nanocomposites exhibit more liquid-like viscoelastic behavior, which matches the results of complex viscosity and storage modulus. It can be observed that PS/M-ATP (3 wt %) nanocomposites exhibit lower tanδ than that of pristine PS, and such a decrease in loss factor is more significant at low frequency. This might arise from the compact hybrid network in nanocomposites that increases the solid-like viscoelastic behavior in a given frequency range.

CONCLUSIONS

In this work, both ATP and functionalized ATP were incorporated into PS by *in situ* suspension polymerization. The effects of functionalized ATP on nanocomposites such as morphology of fracture surface, mechanical properties, thermal stability, and rheological behavior were performed and compared. It was remarkable that M-ATP can enhance the mechanical properties and thermal stability of nanocomposites effectively due to the stronger interfacial bonding. For the nanocomposites containing 3 wt % M-ATP, the formation of hybrid networks in the nanocomposites increased the solid-like behavior significantly, which resulted in higher complex viscosity, storage modulus, and lower loss factor of PS/M-ATP nanocomposites, as compared with the pristine PS and PS/ATP nanocomposites.

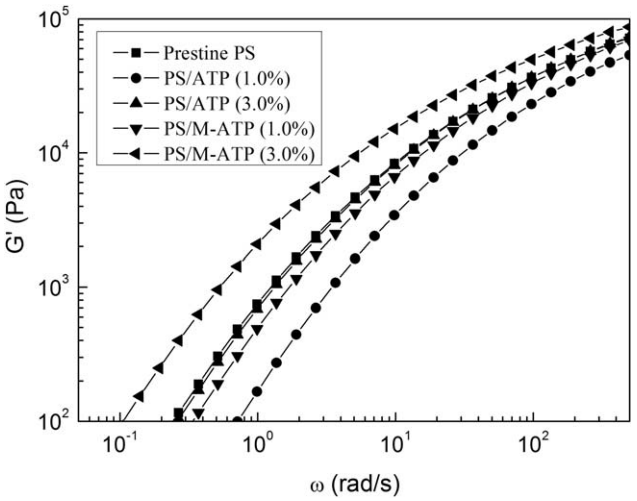

Figure 10. Dependence of storage modulus on frequency for pristine PS and nanocomposites.

ACKNOWLEDGMENTS

This work was financially supported by the Project Funded by the Priority Academic Program Development of Jiangsu Higher Education Institutions (PAPD).

REFERENCE

1. Su, C. H.; Chiu, Y. P.; Teng, C. C.; Chiang, C. L. *J. Polym. Res.* **2010**, *17*, 673.
2. Yang, K.; Gu, M. Y.; Guo, Y. P.; Pan, X. F.; Mu, G. H. *Carbon* **2009**, *47*, 1723.
3. Spitalsky, Z.; Tasis, D.; Papagelis, K.; Galiotis, C. *Prog. Polym. Sci.* **2010**, *35*, 357.
4. Zhang, Y.; Yu, J. R.; Zhou, C. J.; Chen, L.; Hu, Z. M. *Polym. Compos.* **2010**, *31*, 684.
5. Wu, Z. F.; Xue, M.; Wang, H.; Tian, X. Y.; Ding, X.; Zheng, K.; Cui, P. *Polymer* **2013**, *54*, 3334.
6. Yin, H.; Chen, H. F.; Chen, D. J. *J. Mater. Sci.* **2010**, *45*, 2372.
7. Karsli, N. G.; Aytac, A. *Compos. Part B-Eng.* **2013**, *51*, 270.
8. Ma, P. C.; Mo, S. Y.; Tang, B. Z.; Kim, J. K. *Carbon* **2010**, *48*, 1824.
9. Tabari, H. Z.; Nourbakhsh, A.; Ashori, A. *Polym. Eng. Sci.* **2011**, *51*, 272.
10. Zhao, G.; Wang, T. M.; Wang, Q. H. *Polym. Compos.* **2011**, *32*, 1726.
11. Han, W. S. *Polym. Compos.* **2013**, *34*, 156.
12. Lee, C.; Jo, S. M.; Choi, J.; Baek, K. Y.; Truong, Y. B.; Kyrazis, L. L.; Shul, Y. G. *J. Mater. Sci.* **2013**, *48*, 3665.

13. Chan, M. L.; Lau, K. T.; Wong, T. T.; Ho, M. P.; Hui, D. *Compos. Part B-Eng.* **2011**, *42*, 1708.
14. Sahoo, N. G.; Rana, S.; Cho, J. W.; Li, L.; Chan, S. H. *Prog. Polym. Sci.* **2010**, *35*, 837.
15. Rybak, A.; Boiteux, G.; Melis, F.; Seytre, G. *Compos. Sci. Technol.* **2010**, *70*, 410.
16. Costache, M. C.; Heidecker, M. J.; Manias, E.; Wikie, C. A. *Polym. Advan. Technol.* **2006**, *17*, 764.
17. Ou, C. F.; Hsu, M. C. *J. Polym. Res.* **2007**, *14*, 373.
18. Xu, Z.; Gao, C. *Macromolecules* **2010**, *43*, 6716.
19. Fabbri, P.; Bassoli, E.; Bon, S. B.; Valentini, L. *Polymer* **2012**, *53*, 897.
20. Nagamine, S.; Ishimaru, S.; Taki, K.; Ohshima, M. *Mater. Lett.* **2011**, *65*, 3027.
21. Morselli, D.; Bondioli, F.; Fiorini, M.; Messori, M. *J. Mater. Sci.* **2012**, *47*, 7003.
22. Okada, A.; Kawasumi, M.; Kurauchi, T.; Kamigaito, O. *Polym. Prepr.* **1987**, *28*, 447.
23. Kojima, Y.; Usuki, A.; Kawasumi, M.; Okada, A.; Kurauchi, T.; Kamigaito, O. *J. Polym. Sci. Pol. Chem.* **1993**, *31*, 983.
24. Moreno, M.; Ana, M. A. S.; Gonzalez, G.; Benavente, E. *Electrochim. Acta* **2010**, *55*, 1323.
25. Oliveria, C. F. P.; Carastan, D. J. *Polym. Eng. Sci.* **2008**, *48*, 1511.
26. Jaymand, M. *J. Polym. Res.* **2011**, *18*, 957.
27. Liu, S. P.; Huang, I. J.; Chang, K. C.; Yeh, J. M. *J. Appl. Polym. Sci.* **2010**, *115*, 288.
28. Simons, R.; Qiao, G. G.; Bateman, S. A.; Zhang, X. Q.; Lynch, P. A. *Chem. Mater.* **2011**, *23*, 2303.
29. Wang, Z.; Du, X. H.; Yu, H. O.; Jiang, Z. W.; Liu, J.; Tang, T. *Polymer* **2009**, *50*, 5794.
30. Bradley, W. F. *Am. Mineral.* **1940**, *25*, 405.
31. Guggenheim, S.; Adams, J. M.; Bain, D. C.; Bergaya, F.; Brigatti, M. F.; Drits, V. A.; Formso, M. L. L.; Galan, E.; Kogure, T.; Stanjek, H. *Clay Miner.* **2006**, *54*, 761.
32. Guerra, D. L.; Silva, E. M.; Airoldi, C. *Process Saf. Environ.* **2010**, *88*, 53.
33. Tian, H. J.; Guo, Q. J.; Xu, D. Y. *J. Power Sources* **2010**, *195*, 2136.
34. Wang, L.; Zhang, J. P.; Wang, A. Q. *Desalination* **2011**, *266*, 33.
35. Wang, C. H.; Auad, M. L.; Marcovich, N. E.; Nutt, S. *J. Appl. Polym. Sci.* **2008**, *109*, 2562.
36. Qi, X. H.; Liu, M. Z.; Zhang, F.; Chen, Z. B. *Polym. Eng. Sci.* **2009**, *49*, 182.
37. Zhang, Y.; Shen, J.; Li, Q.; Xu, Z. S.; Yeung, K. W. K.; Yi, C. F.; Zhang, Q. Y. *Polym. Compos.* **2013**, *35*, 86.
38. Liu, Y. S.; Liu, P.; Su, Z. X. *J. Disper. Sci. Technol.* **2008**, *29*, 478.
39. Yang, L. Y.; Song, R. F.; Sheng, J. *Chin. Plast.* **2002**, *16*, 47.
40. Sarac, A. S. *Prog. Polym. Sci.* **1999**, *24*, 1149.
41. Zheng, Z. H.; Li, W. J.; Sun, H. M.; Cheng, Z. Q.; Yan, J. T.; Wang, H. Y.; Cui, X. *J. Polym. Compos.* **2013**, *34*, 1110.
42. Guo, Z. Y.; Xing, R. G.; Liu, S.; Yu, H. H.; Wang, P. B.; Li, C. P.; Li, P. C. *Bioorg. Med. Chem. Lett.* **2005**, *15*, 4600.
43. Issa, R. M.; Khedr, A. M.; Rizk, H. *J. Chin. Chem. Soc-TAIP* **2008**, *55*, 875.
44. Wang, R. G.; Li, Z.; Wang, Y. M.; Liu, W. B.; Deng, L. B.; Jiao, W. C.; Yang, F. *Polym. Compos.* **2013**, *34*, 22.
45. Frost, R. L.; Mendelovici, E. *J. Colloid Interf. Sci.* **2006**, *294*, 47.
46. Truica-Marasescu, F.; Wertheimer, M. R. *Plasma Process. Polym.* **2008**, *5*, 44.
47. Beamson, G.; Briggs, D. *Mol. Phys.* **1992**, *76*, 919.
48. Graf, N.; Yegen, E.; Gross, T.; Lippitz, A.; Weigel, W.; Krakert, S.; Terfort, A.; Unger, W. E. S. *Surf. Sci.* **2009**, *603*, 2849.
49. Shard, A. G.; Whittle, J. D.; Beck, A. J.; Brookes, P. N.; Bullett, N. A.; Talib, R. A.; Mistry, A.; Barton, D.; McArthur, S. L. *J. Phys. Chem. B* **2004**, *108*, 12472.
50. Nayak, R. R.; Lee, K. Y.; Shanmugharaj, A. M.; Ryu, S. H. *Eur. Polym. J.* **2007**, *46*, 4916.
51. Li, P.; Zhang, J. P.; Wang, A. Q. *Macromol. Mater. Eng.* **2007**, *292*, 962.
52. Zhang, J. P.; Wang, Q.; Wang, A. Q. *Carbohyd. Polym.* **2007**, *68*, 367.
53. Yin, H.; Chen, H. F.; Chen, D. J. *Colloid. Surface A* **2010**, *367*, 52.
54. Mackay, M. E.; Dao, T. T.; Tuteja, A.; Ho, D. L.; Vanhorn, B.; Kim, H. C.; Hawker, C. J. *Nat. Mater.* **2003**, *2*, 762.
55. Wang, X. L.; Gao, Y.; Mao, K. M.; Xue, G.; Chen, T. H.; Zhu, J. J.; Li, B. H.; Sun, P. C.; Jin, Q. H.; Ding, D. T. *Macromolecules* **2006**, *39*, 6653.
56. Zhang, Q. H.; Fang, F.; Zhao, X.; Li, Y. Z.; Zhu, M. F.; Chen, D. J. *J. Phys. Chem.* **2008**, *112*, 12606.